

# Solar magnetic flux tube simulations with time-dependent ionization

D. E. Fawzy,<sup>1</sup>★ M. Cuntz<sup>2</sup>★ and W. Rammacher<sup>3</sup>★

<sup>1</sup>Faculty of Engineering and Computer Sciences, Izmir University of Economics, Izmir 35330, Turkey

<sup>2</sup>Department of Physics, University of Texas at Arlington, Box 19059, Arlington, TX 76019, USA

<sup>3</sup>Kiepenheuer-Institut für Sonnenphysik, Schöneckstr. 6, 79104 Freiburg, Germany

Accepted 2012 August 1. Received 2012 July 23; in original form 2012 June 12

## ABSTRACT

In the present work we expand the study of time-dependent ionization previously identified to be of pivotal importance for acoustic waves in solar magnetic flux tube simulations. We focus on longitudinal tube waves (LTW) known to be an important heating agent of solar magnetic regions. Our models also consider new results of wave energy generation as well as an updated determination of the mixing length of convection now identified as 1.8 scale heights in the upper solar convective layers. We present 1D wave simulations for the solar chromosphere by studying tubes of different spreading as a function of height aimed at representing tubes in environments of different magnetic filling factors. Multilevel radiative transfer has been applied to correctly represent the total chromospheric emission function. The effects of time-dependent ionization are significant in all models studied. They are most pronounced behind strong shocks and in low-density regions, i.e. the middle and high chromosphere. Concerning our models of different tube spreading, we attained pronounced differences between the various types of models, which were largely initiated by different degrees of dilution of the wave energy flux as well as the density structure partially shaped by strong shocks, if existing. Models showing a quasi-steady rise of temperature with height are obtained via monochromatic waves akin to previous acoustic simulations. However, longitudinal flux tube waves are identified as insufficient to heat the solar transition region and corona in agreement with previous studies.

**Key words:** hydrodynamics – MHD – shock waves – waves – Sun: chromosphere – Sun: surface magnetism.

## 1 INTRODUCTION

The outer atmospheric activity of the Sun as well as other late-type stars is largely determined by the structure and time evolution of photospheric magnetic fields. These fields extend into the stellar outer atmospheres, where they cause non-radiative energy to be deposited (e.g. Anderson & Athay 1989; Linsky 1991; Schrijver 2001; Bogdan et al. 2003; Musielak 2004; Roberts 2004; Ulmschneider & Musielak 2004). This energy is distributed over the chromosphere, transition region and corona; it is also considered pivotal for the heating and acceleration of solar and stellar winds. For new observations and simulations of the relative importance of acoustic and magnetic energy deposition in the solar chromosphere, see e.g. Fossum & Carlsson (2005), Cuntz, Rammacher & Musielak (2007), Kalkofen (2007) and Bello González et al. (2009). Recent joint observational and theoretical studies aimed at elucidating the significance of wave heating in the solar photosphere and lower chromosphere were given by Beck & Rammacher (2010),

Beck, Rezaei & Puschmann (2012) and Wedemeyer-Böhm et al. (2012). The latter study investigates the channelling of magnetic energy through the solar chromosphere into the corona, thus resembling super-tornadoes under solar conditions. Notable reviews aimed at solar chromospheric and coronal heating were given by Narain & Ulmschneider (1996), Klimchuk (2006) and Erdélyi & Ballai (2007).

Magnetic flux tubes are an important feature of the solar surface structure (e.g. Spruit & Roberts 1983; Solanki 1996; Schrijver & Zwaan 2000). Both observational and theoretical studies showed that they are carriers of longitudinal tube waves (LTW; e.g. Herbold et al. 1985; Solanki & Roberts 1992; Hasan & van Ballegoijen 2008), which give rise to considerable temperature increases as a function of height as revealed by chromospheric spectral features. In this paper, we continue to pursue our previous line of research focused on the generation of different types of waves (e.g. Narain & Ulmschneider 1996), effects of the propagation and dissipation of waves (e.g. Herbold et al. 1985; Fawzy, Ulmschneider & Cuntz 1998; Cuntz et al. 1999) and the emergence of chromospheric emission (e.g. Cuntz et al. 1999; Fawzy et al. 2002; Rammacher & Cuntz 2003). However, in accord with previous simulations of acoustic waves (e.g. Carlsson & Stein 1992, 1995; Rammacher &

\*E-mail: diaa.gadelmavla@izmirkonomi.edu.tr (DEF); cuntz@uta.edu (MC); wrammacher@online.de (WR)

Ulmschneider 2003; Rammacher & Cuntz 2005b; Cuntz et al. 2007), the described longitudinal wave simulations will also employ time-dependent (i.e. non-instantaneous) ionization. The geometrical and thermodynamic properties of the tube atmospheres are expected to also impact the dissipation of the wave energy as well as the so-called energy velocity as recently pointed out by Worrall (2012). Time-dependent ionization entails that, e.g. behind strong shocks, the long time-scales of hydrogen ionization/recombination initially prevent the dissipated energy to be converted into ionization energy, thus leading to strong temperature spikes as well as a variety of other dynamic phenomena.

There exists a great motivation to revisit the dissipation of acoustic and magnetic waves in the solar chromosphere, which is the new determination of the mixing length near the top of the solar convective zone. Stein et al. (2009a,b) who provided new state-of-the-art simulations of the solar convection zone on the scale of supergranules, extending 10 per cent of its depth but half of its pressure scale height, deduced a mass mixing length of  $\alpha_{\text{ML}} = 1.8$ , thus superseding the previous results of 1.5 or 2.0 (Steffen 1993; Trampedach et al. 1997), which were widely used in previous solar heating computations.

In our study we will also consider the relevance of tube spreading, i.e. different tube opening radii, for the energetics and thermodynamics of the magnetically heated solar chromospheric structure. Early results based on adiabatic longitudinal waves without the consideration of time-dependent ionization have been given by Fawzy et al. (1998). They found that the tube shape is of critical importance for the heating of flux tubes. In fact, tubes of wide opening radii show little heating, whereas narrow constant cross-section tubes show very large heating at all heights. Previous simulations of longitudinal waves for solar coronal tube structure have been given by e.g. Ofman, Nakariakov & DeForest (1999), Ofman, Nakariakov & Sehgal (2000) and Cuntz & Suess (2004). These results further highlight the importance of tube spreading with respect to the shock wave amplitude and the time-dependent and height-dependent heating rate. Concerning the formation of Ca II and Mg II emission, we will consider a two-component (magnetic and acoustic) model of the solar chromosphere with heating by LTW inside the flux tubes and heating by acoustic waves outside the flux tubes.

The governing equations as well as the methods of our study, including the computation of the initial flux tube models, are discussed in Section 2. In Section 3, we describe the results of our longitudinal wave simulations for solar flux tube models with different tube spreadings; the latter correspond to different magnetic filling factors. The focus of these studies concerns the effects of time-dependent ionization. Our summary and conclusions are given in Section 4.

## 2 METHODS

### 2.1 Theoretical approach

In the following, we summarize some of the key equations with focus on longitudinal magnetohydrodynamic (MHD) tube waves propagating along the vertically directed magnetic flux tubes. Following previous work by e.g. Herbold et al. (1985), the equations to be solved in the Euler frame for continuous 1D flows are given as

$$\frac{\partial \rho A}{\partial t} + \frac{\partial \rho u A}{\partial x} = 0, \quad (1)$$

$$\frac{\partial u}{\partial t} + u \frac{\partial u}{\partial x} + \frac{1}{\rho} \frac{\partial p}{\partial x} + g(x) = 0, \quad (2)$$

$$\frac{\partial S}{\partial t} + u \frac{\partial S}{\partial x} = \left. \frac{dS}{dt} \right|_{\text{rad}}, \quad (3)$$

$$\Phi = A \cdot B = \text{const.}, \quad (4)$$

$$\frac{B^2}{8\pi} + p = p_e = \epsilon p. \quad (5)$$

Here all variables have their usual meaning. Note that  $p$  and  $p_e$  are the gas pressures inside and outside the tube, respectively,  $B$  is the magnetic field strength and  $\epsilon = p_e/p$  denotes the pressure ratio between outside and inside of the tube. Furthermore, the cross-section  $A$  is time dependent owing to the distensibility of the tube (e.g. Lighthill 1978). Moreover, equations (4) and (5) represent the conservation of the magnetic flux  $\Phi$  and the horizontal pressure balance between inside and outside the tube, respectively. All quantities are both functions of height  $x$  and time  $t$ ; strictly speaking, this also applies to  $p_e$  where we however assume  $p_e = p_e(x)$  in accord to previous studies (e.g. Herbold et al. 1985; Cuntz et al. 1999), as we do not consider the effects of the time dependency of the outside medium towards the tube.

Similar to the case of acoustic waves (e.g. Ulmschneider et al. 1977; Cuntz & Ulmschneider 1988), the system of equations can be transformed into its characteristic form as pursued in detail by Rammacher & Ulmschneider (2003). A key equation concerns the behaviour of the thermodynamic variables along the  $C^0$  characteristics with the relevant compatibility relation given as

$$dS = \left. \frac{dS}{dt} \right|_{\text{rad}} dt, \quad (6)$$

which can also be written as

$$dT - \left( \frac{\partial T}{\partial p} \right)_S dp - \left( \frac{\partial T}{\partial S} \right)_p \left. \frac{dS}{dt} \right|_{\text{rad}} dt = 0. \quad (7)$$

Note that e.g.  $(\partial T / \partial p)_S$  and  $(\partial T / \partial S)_p$  constitute well-known thermodynamic relationships (e.g. Mihalas & Mihalas 1984); they need to be solved numerically if deviations from the thermodynamic equilibrium, as in the case of our study, are considered.

The rate equations for the general case of flows have been discussed in detail by e.g. Mihalas & Mihalas (1984) and have been implemented into actual OHD/MHD codes<sup>1</sup> by Carlsson & Stein (2002) and Rammacher & Ulmschneider (2003), among others. Assuming a simplified hydrogen atom of  $N = 3$  levels, namely two bound levels plus the continuum level, while considering radiative processes  $R$  and collisional processes  $C$ , the population density of level  $i$  can be obtained through solving

$$\frac{\partial n_i}{\partial t} + \frac{\partial n_i u}{\partial x} = \sum_{j=1 \wedge j \neq i}^N (n_j P_{ji} - n_i P_{ij}), \quad (8)$$

where  $P_{lk}$  denotes the rate of transitions (per  $\text{cm}^3$  and s) taking place from level  $l$  to level  $k$  and  $P_{lk} = R_{lk} + C_{lk}$ . This equation represents the conservation equation for the particle number density  $n_i$ ; however, it also takes into account the generation and destruction of  $n_i$  caused by transitions from and to other levels<sup>2</sup>. The LHS

<sup>1</sup> OHD = Ordinary Hydrodynamics.

<sup>2</sup> Equation (8) is in line with the earlier work by Rammacher & Ulmschneider (2003). In Carlsson & Stein (2002) based on a six-level atom it was shown that hydrogen ionization goes with collisional excitation to  $n = 2$ , then with radiative ionization to the continuum, a pattern broadly consistent with the present study. On the other hand, Carlsson & Stein (2002) found that recombination transitions occur by going from the continuum level to excited levels with  $n > 2$ , which is not possible in the three-level atom selected.

of equation (8) would be zero if the particles of species  $i$  were conserved; in this case, equation (8) would represent the standard continuity equation for particles of species  $i$ .

If time-dependent (i.e. non-instantaneous) ionization processes are considered, the change in the population density for the continuum level is given as

$$\frac{dn_c}{dt} = \sum_{i=1}^{N-1} n_i (R_{ic} + C_{ic}) - n_c \sum_{i=1}^{N-1} (R_{ci} + C_{ci}) - n_c W \quad (9)$$

(Rammacher & Ulmschneider 2003); the latter also requires the time-dependent solution of the advection term given as

$$W = \rho \left( \frac{\partial T}{\partial p} \right)_s \frac{dS}{dt} \Big|_{\text{rad}} - \frac{1}{\rho c_s^2} \frac{dp}{dt}, \quad (10)$$

where  $c_s$  denotes the adiabatic sound speed given as

$$c_s = \left[ \left( \frac{\partial p}{\partial \rho} \right)_s \right]^{1/2} = \left[ \left( \frac{\partial \rho}{\partial p} \right)_T + \left( \frac{\partial \rho}{\partial T} \right)_p \left( \frac{\partial T}{\partial p} \right)_s \right]^{-1/2}. \quad (11)$$

The number density of the hydrogen continuum population is closely related to the electron density  $n_e$ , which is of critical importance for the manifestation of the chromospheric radiative emission function (e.g. Vernazza, Avrett & Loeser 1981; Avrett 1985). Other equations concern the conservation of the total number of hydrogen particles,  $n_{\text{tot}}$ , given as

$$\frac{1 + Z_{\text{el}}}{X_{\text{el}}} \sum_{i=1}^{N-1} n_i + \left( 1 + \frac{1 + Z_{\text{el}}}{X_{\text{el}}} \right) n_c = \frac{p}{kT} = n_{\text{tot}}, \quad (12)$$

and the conservation of electrons given as

$$n_e = \left( 1 + \frac{Z_{\text{el}}}{X_{\text{el}}} \right) n_c + \frac{Z_{\text{el}}}{X_{\text{el}}} \sum_{i=1}^{N-1} n_i, \quad (13)$$

where  $X_{\text{el}}$  and  $Z_{\text{el}}$  denote the element abundances of hydrogen and the metals, respectively. Note that  $p$  is the gas pressure,  $T$  is the temperature and  $k$  is Boltzmann's constant.

## 2.2 Comments on the (magneto-)hydrodynamic computer code

The treatment of acoustic and longitudinal flux tube waves concerning solar and stellar chromospheric models is pursued based on the code by Rammacher & Ulmschneider (2003) and subsequent augmentations by Rammacher & Cuntz (2005b). This code is suitable for the simulation of 1D wave propagation and dissipation and, moreover, also allows the treatment of time-dependent (i.e. non-instantaneous) ionization processes for hydrogen and other elements by obtaining solutions of the time-dependent statistical rate equations (see also Carlsson & Stein 1992, 1995). Additional features of the code encompass the evaluation of the radiative losses (and gains) by also taking into account departures from local thermodynamic equilibrium. Shocks are treated as discontinuities based on adequate solutions of the Rankine–Hugoniot relations; see e.g. previous work by Nieuwenhuijzen et al. (1993) for a quasi-analytic method for the computation of the thermodynamic relationships across shocks in the presence of radiative and ionization processes.

The adopted methods are suitable for the treatment of both monochromatic and spectral waves. In the framework of our models, time-dependent ionization is considered with respect to hydrogen as well as magnesium and calcium. Regarding the chromospheric emission losses, we provide a detailed treatment of the Ca II K and Mg II k lines; the total chromospheric emission losses are obtained

via appropriate scaling, see e.g. Cuntz et al. (1999) for previous applications of this approach. The scaling factors have been determined by inspecting representative solutions of the wave models and by applying multilevel radiative transfer computations with MULTI (see Rammacher et al. 2005). Radiative transfer in the continuum, notable H<sup>-</sup>, is pursued following the method of Schmitz, Ulmschneider & Kalkofen (1985). Another important aspect of our calculations is the implementation of boundary conditions. At the top boundary, a transmitting boundary condition is used, whereas at the bottom boundary, the injection of the magnetic or acoustic wave energy flux is simulated via a piston-type boundary condition; the latter is suitable for monochromatic waves as well as acoustic and LTW frequency spectra (see Rammacher & Ulmschneider 2003, and references therein for details).

## 2.3 Wave energy fluxes and wave energy spectra

The wave energy fluxes and wave energy spectra are calculated following the approach by Musielak et al. (1994) and Ulmschneider, Theurer & Musielak (1996); see also Fawzy & Cuntz (2011) for updated results pertaining to a grid of models for a set of main-sequence stars including the Sun. These types of models incorporate a detailed description of the spatial and temporal spectrum of the turbulent flow to obtain adequate results for the frequency integrated acoustic energy fluxes along with the wave frequency spectra; furthermore, they utilize an extended Kolmogorov spectrum with a modified Gaussian frequency factor. Both the acoustic and magnetic wave energy fluxes depend on the mixing-length parameter  $\alpha_{\text{ML}}$ , for which  $\alpha_{\text{ML}} = 1.8$  is used (Stein et al. 2009a,b).

According to the updated value of  $\alpha_{\text{ML}}$ , the initial wave energy flux for the acoustic model is given as  $F_{\text{M}} = 1.09 \times 10^8 \text{ erg cm}^{-2} \text{ s}^{-1}$  (Ulmschneider et al. 1996), see Table 1. For the wave energy flux of the longitudinal flux tube wave, we use  $F_{\text{M}} = 2.80 \times 10^8 \text{ erg cm}^{-2} \text{ s}^{-1}$  (Fawzy & Cuntz 2011); this value assumes a pressure ratio between outside and inside of the tube of  $\epsilon = 3$  (see equation 5). It is based on the assumption of an inside magnetic field strength of 1700 G, noting that in our model the equipartition magnetic field strength is given as  $B_{\text{eq}} = \sqrt{8\pi p_e} = 2082 \text{ G}$  with  $B/B_{\text{eq}} \simeq 0.82$ . The adopted inside tube magnetic field strength has been taken at an optical depth of  $\tau_{5000} = 1.3$ , corresponding to a mass column density of  $2.1 \text{ g cm}^{-2}$ . It is found that the longitudinal wave energy flux is increased relative to the acoustic energy flux by a factor of 2–3.5, depending on the mixing-length parameter  $\alpha_{\text{ML}}$ , owing to decisive differences in the turbulent velocity  $u_t$ , which is considerably enhanced in the magnetic case (e.g. Ulmschneider & Musielak 1998).

For previous elaborations on the appropriate value for  $F_{\text{M}}$  and  $B_{\text{eq}}$ , see e.g. Ulmschneider, Musielak & Fawzy (2001). Detailed studies of magnetic field strengths for solar flux tubes have been given by e.g. Stenflo (1978) and Solanki (1993), allowing us to motivate our choice of  $B_{\text{eq}}$ . Information on the wave frequency spectra for

**Table 1.** Acoustic and LTW energy generation.

$\alpha_{\text{ML}}$	Acoustic		LTW	
	$u_t$ (cm s <sup>-1</sup> )	$F_{\text{M}}$ (erg cm <sup>-2</sup> s <sup>-1</sup> )	$u_t$ (cm s <sup>-1</sup> )	$F_{\text{M}}$ (erg cm <sup>-2</sup> s <sup>-1</sup> )
1.5	$5.50 \times 10^4$	$5.48 \times 10^7$	$1.22 \times 10^5$	$1.95 \times 10^8$
1.65	$6.81 \times 10^4$	$7.85 \times 10^7$	$1.25 \times 10^5$	$2.48 \times 10^8$
1.8	$8.63 \times 10^4$	$1.09 \times 10^8$	$1.31 \times 10^5$	$2.80 \times 10^8$
2.0	$1.09 \times 10^5$	$1.54 \times 10^8$	$1.35 \times 10^5$	$3.02 \times 10^8$

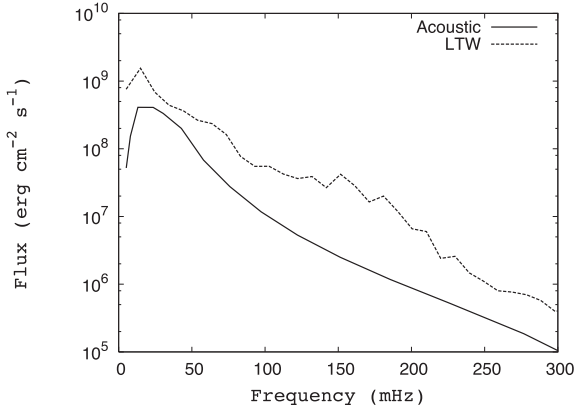


**Figure 1.** Depiction of the generated flux for acoustic waves (solid) and longitudinal flux tube waves (dashed) as a function of frequency for a mixing length of  $\alpha_{ML} = 1.8$ . For the magnetic waves we consider the model with a bottom magnetic field strength of 1700 G.

longitudinal flux tube waves was presented by e.g. Ulmschneider & Musielak (1998) and Ulmschneider et al. (2001), see Fig. 1 for the spectral wave energy distribution serving as basis for our models<sup>3</sup>. These authors found that the spectral energy distribution for both the acoustic and longitudinal frequency spectrum has a maximum close to a wave period of 60 s. We will use this value in conjunction with the monochromatic wave models of our study.

There is also considerable previous work on the most appropriate value for the initial wave energy flux of LTW; the latter is also modestly affected by the solar photospheric opacities owing to their influence on the construction of the solar tube models (i.e. attainment of radiative equilibrium, position of optical depth  $\tau_{5000}$ ). Previous work by Ulmschneider et al. (2001) adopted the opacity tables compiled by Bohn (1984) and Ulmschneider et al. (1996), whereas more recent simulations (Fawzy 2010) use the opacity table given by R. L. Kurucz and collaborators (see Castelli & Kurucz 2004 for details).

This latter approach is adopted in this paper. In principle, the opacity table by R. L. Kurucz and collaborators yields noticeably lower initial wave energy fluxes, which for  $\alpha_{ML}$  between 1.8 and 2.0 are reduced by typically 30 per cent compared to the models based on the opacity table considered by Ulmschneider et al. (2001). A relatively high initial wave energy flux based on  $\alpha_{ML} = 2.0$  was also adopted by Rammacher & Cuntz (2005a), which is a further reason for revisiting the propagation and dissipation of LTW in the Sun by considering an advanced treatment of the hydrodynamic and thermodynamic features as well as a realistic initial wave energy flux. Future investigations of stellar convection and photospheres may also be based on the massively parallel recently developed code BIFROST (Gudiksen et al. 2011), which is designed to simulate stellar atmospheres from the convection zone to the corona.

<sup>3</sup> The longitudinal wave energy spectrum as obtained through the study of non-linear time-dependent responses of theoretical solar flux tubes to external pressure fluctuations (e.g. Ulmschneider & Musielak 1998) is found to be somewhat bumpy, which is a consequence of the occurrence of large-amplitude perturbations (i.e. spiky waves) that are still apparent after temporal averaging has been applied.

## 2.4 Flux tube models

For our models we consider three different flux tube geometries characterized by different amounts of spreading as a function of height; see e.g. Rammacher & Ulmschneider (1989) and Fawzy et al. (1998) for previous work on the effects of tube spreading on the deposition of non-radiative energy and the formation of chromospheric emission with focus on the Sun. The bottom radii of the tube models are chosen as 55 km corresponding to half of the photospheric pressure scale-height; note that the base pressure of the tubes is closely aligned to the VAL-C model (Vernazza et al. 1981). We also assume a magnetic field strength at the bottom of the tubes of  $B_0 = 1700$  G informed by previous studies (Fawzy et al. 1998). We again consider wine-glass shaped tubes with top opening radii of 150, 700 and 1500 km, respectively (see Table 2). For these tubes, exponential spreading is assumed at relatively low heights, followed by linear spreading. Full spreading is attained at heights of 571, 1126 and 1639 km, respectively; see Fig. 2 for a depiction of the adopted tube models.

The tube with a top opening radius of 700 km has a top opening area approximately 20 times larger than the tube with 150 km. Moreover, the difference in the opening areas between the wine-glass tubes with opening radii of 700 and 1500 km is a factor of 4.6. The flux tubes represent regions with magnetic filling factors  $f = r_B^2/r_T^2$  equal to 0.1, 0.01 and 0.001 per cent, respectively, with  $r_B$  and  $r_T$  denoting the base radius and top radius of the tube, respectively. The effect of flux tube spreading results in a progressively lower inside magnetic field strength with a decreasing magnetic filling factor  $f$ , entailing  $B(r_T) = 2.3$  G for  $f = 0.001$  per cent compared to 229 G for  $f = 0.1$  per cent (see Table 2).

**Table 2.** Magnetic tube models.

$f$ (per cent)	$r_B$ (km)	$r_T$ (km)	$B(r_T)$ (G)
0.1	55	150	229
0.01	55	700	10.5
0.001	55	1500	2.3

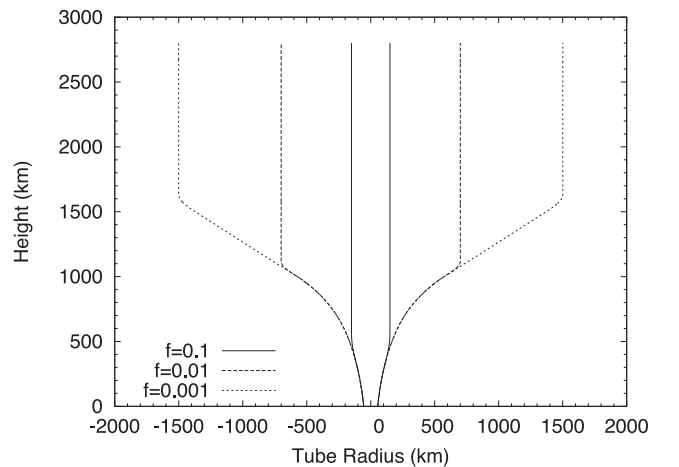


**Figure 2.** Spread of magnetic flux tubes for the different magnetic filling factors.

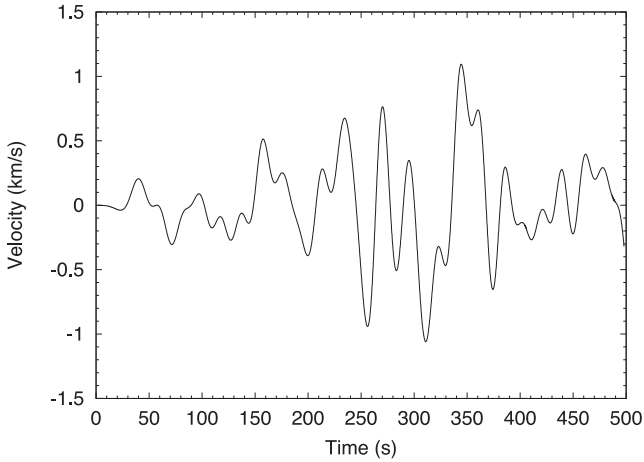


**Figure 3.** Velocity at the bottom boundary of the flux tube models in response to the longitudinal wave energy spectrum.

### 3 RESULTS AND DISCUSSION

#### 3.1 Detailed time-dependent model simulations

By adopting the wave energy flux and wave frequency spectrum for  $\alpha_{ML} = 1.8$ , we pursued detailed simulations for LTW for three different flux tubes (see Section 2.4); in the following, we show calculations pertaining to the magnetic filling factors of  $f = 0.1$  and 0.001 per cent. The stochastic velocity function at the bottom of the tubes owing to the application of the longitudinal wave frequency spectrum is depicted in Fig. 3. Time-dependent ionization (TDI) has been considered for hydrogen as well as for Ca II and Mg II. To demonstrate the structure of our dynamic models in conjunction with the impact of different tube spreadings, we depict snapshots at identical elapsed times, which are 400, 800 and 1400 s (see Fig. 4).

The general behaviour of the depicted waves in these models is characterized by temporal increases of the wave amplitudes resulting in the formation of shocks, typically occurring near 700 and 800 km for  $f = 0.1$  and 0.001 per cent, respectively. The tube geometry determines the general position of the chromospheric temperature rise. It is found that the larger the tube spreading, the greater the height of the temperature rise. In models of negligible tube spreading, the shock amplitudes tend to stay constant or increase as

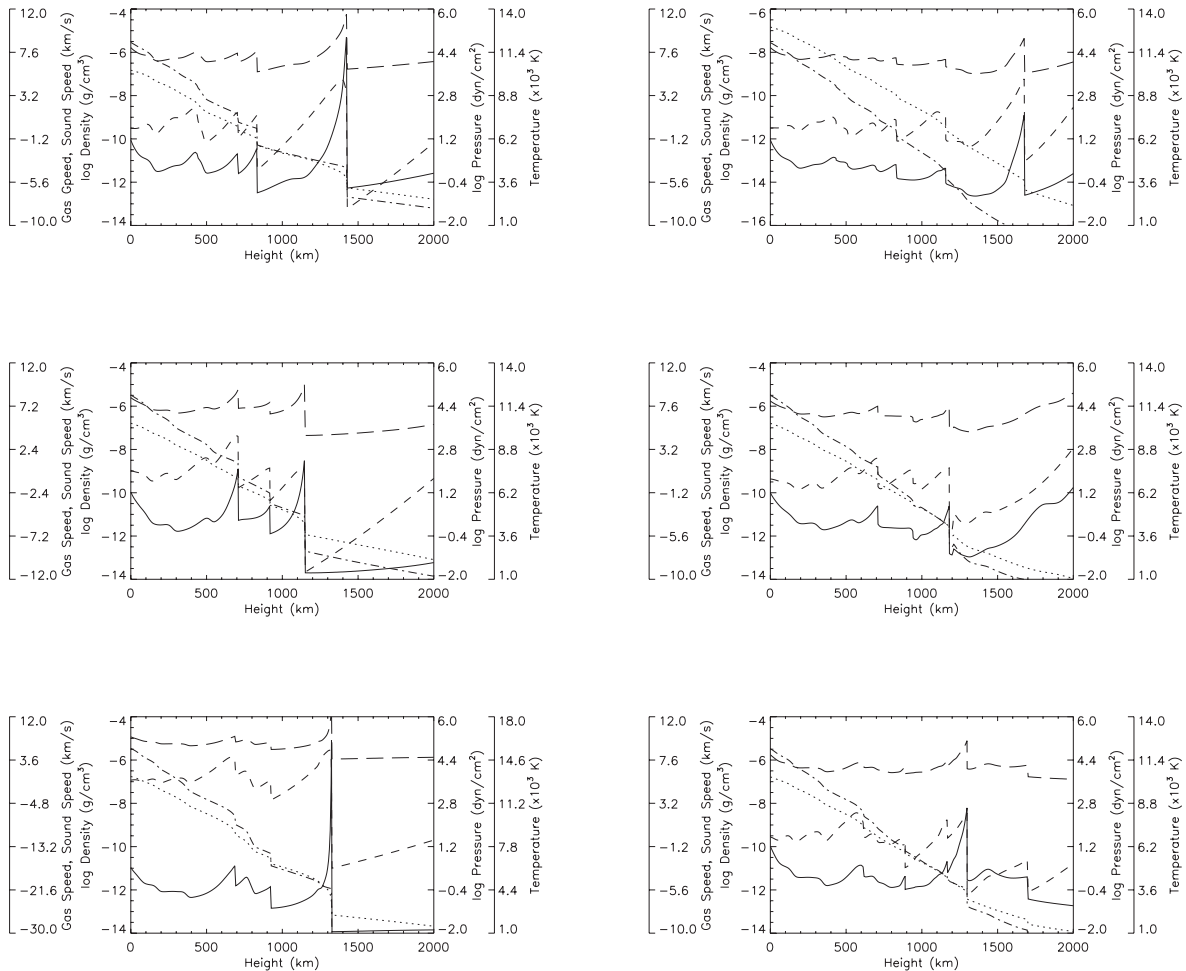


**Figure 4.** Two sequences of snapshots of longitudinal wave computations for magnetic flux tubes with filling factors of  $f = 0.1$  per cent (left-hand column) and  $f = 0.001$  per cent (right-hand column) based on time-dependent ionization and with consideration of frequency spectra. These filling factors correspond to tube opening radii of 150 and 1500 km, respectively. We depict the following variables: temperature (solid lines), gas speed (dashed lines), density (short dashed lines), sound speed (long dashed lines) and gas pressure (dash-dotted lines). The snapshots are taken at times of 400, 800 and 1400 s (top to bottom).

a function of height. However, this behaviour is counteracted by the impact of tube spreading: the larger the spreading of the tube, the greater the area over which the wave energy is distributed (i.e. geometrical dilution), resulting in smaller wave amplitudes (see also Section 3.3).

Both models are shaped by strong interaction of shocks, which leads to increased shock strengths  $M_s$  as a function of height. The shock strength  $M_s$  is given as

$$M_s = \frac{U_{\text{sh}} - u_1}{c_{\text{T1}}}, \quad (14)$$

where  $U_{\text{sh}}$  denotes the shock speed, and  $u_1$  and  $c_{\text{T1}}$  denote the gas speed and tube speed in front of the shock, respectively.

This behaviour is most pronounced for relatively narrow tubes; for example, we find that the main shock at  $t = 1400$  s in the model of  $f = 0.1$  per cent has a strength of 6.62 compared to 1.02 in the model of  $f = 0.001$  per cent. This type of behaviour is also mirrored by the jump in temperature across the shocks. The corresponding post-shock temperatures are typically relatively high at relatively large atmospheric heights and in models of relatively narrow tubes, noting that narrow tubes imply higher shock strengths anyhow and, moreover, entail more intense shock merging. For  $f = 0.1$  per cent at an elapsed time of 1400 s (see Fig. 4), the attained post-shock temperatures range between 4650 and 16 170 K. In models of smaller magnetic filling factors, the post-shock temperatures are typically considerably lower; additionally, the variations in post-shock temperatures for given model simulations and time steps are also reduced. Furthermore, in models of time-dependent ionization, the post-shock temperatures are also considerably higher than in equivalent models without time-dependent ionization, a behaviour consistent with previous acoustic models (e.g. Carlsson & Stein 1992, 1995; Rammacher & Ulmschneider 2003, see also Section 3.2).

Additionally, the occurrence of relatively strong shocks in models of  $f = 0.1$  per cent compared to  $f = 0.001$  per cent results in higher levels of momentum transfer, which typically lead to smaller densities in the top regions of those tubes as well as characteristic behaviours for the time-averaged temperatures (see Section 3.3). Although relatively large gas speeds may be attained by this process, the outflow speeds typically remain subsonic. Additionally, due to energy dissipation and radiative energy losses, the wave energy fluxes considerably decrease with atmospheric height (see Tables 3 and 4). However, comparing tubes of  $f = 0.1$  and 0.001 per cent, the decrease in the wave energy flux with height regarding the tube with  $f = 0.001$  per cent is significantly less than expected from the degree of geometrical dilution. This phenomenon is caused by the relatively low density in the tube with  $f = 0.1$  per cent owing to the action of strong shocks (see Section 3.3); for previous results on adiabatic LTW simulations, see e.g. Fawzy et al. (1998). At a height of 2000 km, the wave energy fluxes are given as  $5.10 \times 10^3$  and  $1.93 \times 10^3$  erg cm<sup>-2</sup> s<sup>-1</sup> for  $f = 0.1$  and 0.001 per cent,

**Table 3.** LTW energy flux: monochromatic waves.<sup>a</sup>

Height (km)	nTDI		TDI	
	$f = 0.1$	$f = 0.001$	$f = 0.1$	$f = 0.001$
600	$1.43 \times 10^7$	$7.48 \times 10^6$	$1.08 \times 10^7$	$1.56 \times 10^6$
900	$2.21 \times 10^6$	$4.15 \times 10^5$	$1.97 \times 10^6$	$1.01 \times 10^5$
1200	$2.62 \times 10^5$	$1.01 \times 10^4$	$2.56 \times 10^5$	$2.79 \times 10^3$
2000	$1.02 \times 10^4$	$3.37 \times 10^3$	$4.87 \times 10^3$	$2.67 \times 10^2$

<sup>a</sup>The LTW energy fluxes are given in erg cm<sup>-2</sup> s<sup>-1</sup>.

**Table 4.** LTW energy flux: spectral waves.<sup>a</sup>

Height (km)	nTDI		TDI	
	$f = 0.1$	$f = 0.001$	$f = 0.1$	$f = 0.001$
600	$1.09 \times 10^7$	$3.24 \times 10^6$	$1.53 \times 10^7$	$3.49 \times 10^6$
900	$2.75 \times 10^6$	$4.90 \times 10^5$	$3.33 \times 10^6$	$5.49 \times 10^5$
1200	$4.30 \times 10^5$	$3.31 \times 10^4$	$5.07 \times 10^5$	$2.58 \times 10^4$
2000	$4.34 \times 10^4$	$5.41 \times 10^3$	$5.10 \times 10^3$	$1.93 \times 10^3$

<sup>a</sup>The LTW energy fluxes are given in erg cm<sup>-2</sup> s<sup>-1</sup>.

respectively (see Table 4) if time-dependent ionization is assumed. For the intermediate models of  $f = 0.01$  per cent (not shown), the wave energy flux at 2000 km is given as  $4.17 \times 10^3$  erg cm<sup>-2</sup> s<sup>-1</sup>. At low chromosphere heights, the heating and energy dissipation rates are identified as almost independent of the magnetic filling factor consistent with observational constraints (Bruls & Solanki 1993).

### 3.2 Effects of flux tube spreading and time-dependent ionization

To obtain further insight into the effect of tube spreading on the atmospheric shock strengths as well as into other features owing to time-dependent ionization we computed a set of detailed models. They include monochromatic wave models without time-dependent ionization as well as models with frequency spectra with and without time-dependent ionization. For each set of models, we considered tube spreadings corresponding to magnetic filling factors of  $f = 0.1$ , 0.01 and 0.001 per cent, respectively, thus allowing us to gauge the impact of tube spreading on the temperature structure and shock strengths.

The first set of models is based on monochromatic waves. For all three tube spreadings we chose an elapsed time of 2500 s, thus ensuring appropriate comparisons between the models. Hence, almost 30 shocks have been inserted into the atmosphere; therefore, all three tube atmospheres have reached a dynamic steady state, i.e. the interaction between the shocks (i.e. ongoing shock merging) has subsided. Comparisons between models of different tube spreading (see Fig. 5, top panel) indicate that the models with narrow tube spreading (i.e. high magnetic filling factor) are characterized by relatively high shock strengths, whereas models with wide tube spreading (i.e. low magnetic filling factor) are shaped by relatively small shock strengths. Specifically, for regions beyond 1200 km, the typical shock strength for  $f = 0.1$  per cent varies between  $M_s = 1.85$  and 2.77, whereas for  $f = 0.001$  per cent, it is usually only  $M_s = 1.60$ . For  $f = 0.01$  per cent, intermediate shock strength values are found, as expected. In models of monochromatic waves the shocks have attained limiting shock strength, which is found to depend on the height-dependent behaviour of the tube spreading, as previously pointed out through analytical means (Cuntz 2004). Previous simulations for solar flux tubes based on adiabatic LTW waves without time-dependent ionization also show a similar kind of behaviour (Fawzy et al. 1998). Due to the omission of detailed time-dependent ionization, it is found that the degree of hydrogen ionization at 2000 km is about 95 per cent for  $f = 0.1$  and 0.01 per cent. For  $f = 0.001$  per cent, a lower value for the hydrogen ionization degree is found; in this case, a smooth and steady increase of the hydrogen ionization degree occurs between 1200 and 2000 km.

The second and third set of models are based on LTW frequency spectra. Fig. 5 (middle and bottom panels) shows snapshots with and without the consideration of time-dependent ionization,

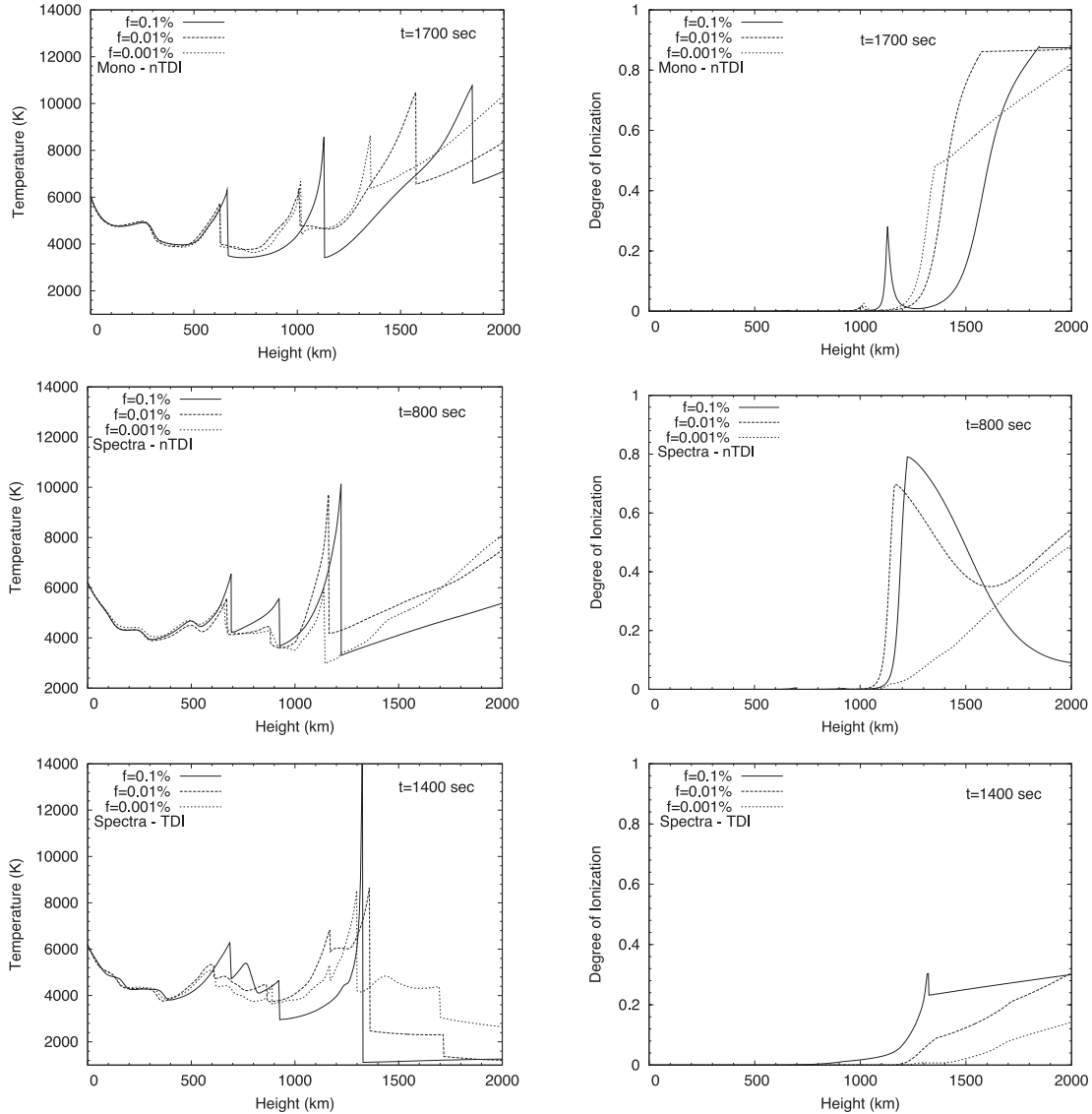


**Figure 5.** Behaviour of the temperature (left-hand column) and hydrogen ionization degree (right-hand column) of propagating longitudinal flux tube waves concerning tube models with different spreadings, which correspond to filling factors of  $f = 0.1$ ,  $0.01$  and  $0.001$  per cent. We depict monochromatic wave models (top) and models with frequency spectra (middle) without time-dependent ionization as well as models with frequency spectra including time-dependent ionization (bottom). Note the vast differences in the temperature amplitudes. The very large temperature spike in the model with  $f = 0.1$  per cent (left-hand column, bottom) reaches  $16\,170$  K.

respectively. For both types of models, we again consider magnetic filling factors of  $f = 0.1$ ,  $0.01$  and  $0.001$  per cent. The snapshots displayed for these sets of models are taken at  $800$  and  $1400$  s, respectively; furthermore, the elapsed time of simulation is about  $2000$  s. The main shocks in Fig. 5 (middle panel), attained through the process of shock merging, have strengths of  $3.19$ ,  $3.18$  and  $2.11$ , respectively. The main shock for  $f = 0.1$  per cent has a post-shock temperature of  $10\,070$  K; the hydrogen ionization degree in front of the shock is  $78$  per cent, and shortly behind the shock it is close to zero. By comparison, the post-shock temperatures of the main shocks pertaining to  $f = 0.01$  and  $0.001$  per cent are  $9250$  and  $6470$  K, respectively, which clearly indicates the impact of tube spreading. Clearly, the change of structure due to different magnetic filling factors is a direct consequence of the dilution of the wave energy flux (see Table 4), including associated magnetohydrodynamic, thermodynamic and radiative phenomena, particularly those associated with the formation of shocks of different strengths. At

heights of  $1200$  km, the wave energy flux is reduced by factors of  $1.5 \times 10^{-3}$ ,  $2.9 \times 10^{-4}$  and  $1.9 \times 10^{-5}$  in tube models with  $f = 0.1$ ,  $0.01$  and  $0.001$  per cent, respectively.

Fig. 5 (bottom panel) reflects a similar setting but now both time-dependent ionization and LTW frequency spectra are taken into account. The main difference to the kind of simulations previously discussed is an enhanced tendency of building up very strong shocks due to shock merging, particularly for the model with a magnetic filling factor of  $0.1$  per cent. In this case, a very large temperature spike with a post-shock temperature of  $16\,170$  K occurs; the corresponding shock strength is given as  $M_s = 6.62$ . In contrast, however, at relatively low heights, a considerable number of small shocks are encountered. Moreover, at heights between  $600$  and  $1000$  km, shock strengths are typically between  $M_s = 1.2$  and  $1.5$  in models of  $f = 0.1$  per cent. The shock strengths are even lower in models with  $0.001$  per cent; in the latter case, the shock formation is postponed to larger heights. The merging of shocks leads to the build-up of

very strong shocks, a process that is significantly amplified in models of time-dependent ionization, owing to the fact that virtually no energy is used immediately behind the shocks to ionize hydrogen (or any other species). Therefore, an increased amount of energy is available to further increase the post-shock temperatures.

The dilution of the wave energy flux is also highly significant in these types of models depending on the degree of geometrical spreading. At heights of 1200 km, the initial wave energy flux is reduced by factors of  $1.8 \times 10^{-3}$ ,  $3.9 \times 10^{-4}$  and  $9.2 \times 10^{-5}$ , in models with  $f = 0.1$ , 0.01 and 0.001 per cent, respectively. However, an assessment of the absolute amount of wave energy flux indicates (see Tables 3 and 4) that it is less diluted than expected from the degree of geometrical dilution, which obviously is a factor of 100 between  $f = 0.1$  and 0.001 per cent. The reason for this type of behaviour is that models with  $f = 0.1$  per cent have a lower overall density; furthermore, in those models there is a higher loss of energy behind the shocks due to enhanced radiative energy losses and the initiation of episodic outflow. For the same reason, the reduction of the wave energy flux with height is also more drastic in models with time-dependent ionization compared to models without consideration of this process (TDI versus nTDI).

For the assortments of small shocks, it is noteworthy that different shock strengths correspond to different shock speeds; therefore, the shocks in models with LTW frequency spectra are poised to overtake one another, thus invoking significant shock merging as well as the build-up of very strong shocks. This result has already been obtained in 1D acoustic models (e.g. Cuntz 1987), and it is evident in 1D LTW models with and without the consideration of time-dependent ionization, but it is drastically enhanced if time-dependent ionization of hydrogen is considered. The occurrence of very strong shocks is a typical feature of the combined influence of frequency spectra and time-dependent ionization inherent in 1D (magneto-) hydrodynamic models, see e.g. Carlsson & Stein (1992) for previous results on acoustic models. Fig. 5 (middle and bottom panels) depicts the behaviour of the hydrogen ionization degree in the various models in front and behind the shocks. Clearly, the hydrogen ionization degrees are progressively lower in models of smaller values of  $f$ ; however, in models without time-dependent ionization of hydrogen it drops to almost zero in the post-shock regions (see Fig. 5, middle panel), whereas in models with time-dependent ionization of hydrogen it is essentially maintained (see Fig. 5, bottom panel).

### 3.3 Behaviour of time-averaged temperatures and ionization degrees

Additional insight into the overall dynamic structure of flux tubes subjected to the propagation and dissipation of LTW can be obtained by assessing the behaviour of time-averaged temperatures. Again, we considered both monochromatic waves and frequency spectra (i.e., spectral waves), while pursuing detailed comparisons for models with and without time-dependent ionization. Concerning monochromatic models, we also pursued computations for acoustic waves aimed at representing atmospheric structure exterior to the flux tubes; in this regard, plane-parallel geometry was assumed. In all types of models, the wave energy generation was derived from a mixing length of  $\alpha_{ML} = 1.8$  resulting in an initial wave energy flux of  $1.09 \times 10^8$  and  $2.80 \times 10^8 \text{ erg cm}^{-2} \text{ s}^{-1}$  for the acoustic and magnetic models, respectively (see Table 1). For the magnetic flux tube simulations, we again considered tube geometry given by magnetic filling factors of  $f = 0.1$ , 0.01 and 0.001 per cent. Exam-

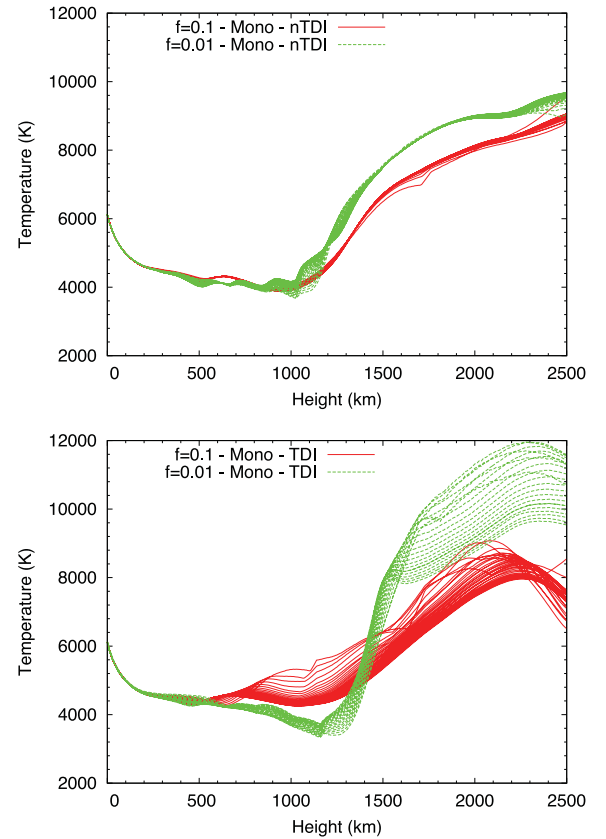


**Figure 6.** Build-up of mean (i.e. time-averaged) temperatures for models with and without time-dependent ionization (bottom and top figure, respectively). Note the influence of the different tube spreadings, denoted as magnetic filling factors  $f = 0.1$  and 0.01 per cent; see Table 2. The time of averaging for the various models is close to 60 s. For the simulations with time-dependent ionization, the averaging starts at 513 s ( $f = 0.1$  per cent) and 821 s ( $f = 0.01$  per cent) and for the simulations without time-dependent ionization, it starts at 607 s ( $f = 0.1$  per cent) and 612 s ( $f = 0.01$  per cent).

ples for the steady build-up of time-averaged temperatures owing to the implemented averaging procedure are conveyed in Fig. 6.

Detailed information on the behaviour of the time-averaged temperatures is given in Fig. 7, which depicts a total of 14 models. Let us first focus on the evaluation of dynamic magnetic flux tube models based on monochromatic waves. Typically, we awaited the insertion of 20 to 50 wave periods into the atmosphere prior to the evaluation of mean (i.e. time-averaged) quantities to ensure that the switch-on behaviour of the tube atmospheres has subsided and dynamic equilibria have been reached. The time-averaged temperatures of the various tube models as well as those of the acoustically heated models are relatively similar at heights below 800 km, although they are found to be highest in the model with the smallest spreading (i.e.  $f = 0.1$  per cent), as expected. This latter result can be understood based on the dilution of the wave energy flux, which also affects the height of shock formation. The latter is given as 400, 550 and 850 km for the models with 0.1, 0.01 and 0.001 per cent, respectively. For the acoustic model, the height of shock formation is given as 600 km. Only minor differences are obtained between models with and without time-dependent ionization, noting that due to the relatively high densities, low temperatures and small shock strengths (if any), the effects due to time-dependent ionization are less pronounced.

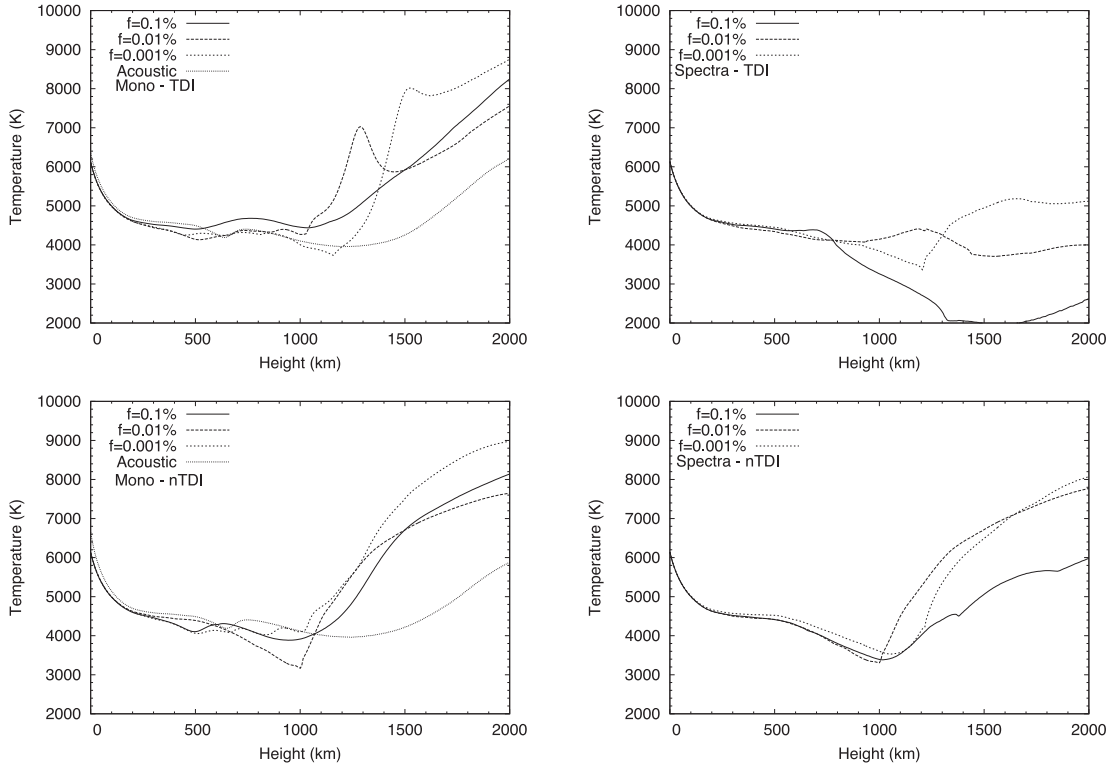


**Figure 7.** Comparison of time-averaged temperatures for longitudinal wave computations pertaining to different types of models. We show models based on monochromatic waves (left-hand column) and frequency spectra (right-hand column). The top and bottom row depicts models with and without consideration of time-dependent ionization, respectively. Concerning the model series based on monochromatic waves, we also show acoustic wave models for comparison. Regarding the magnetic flux tube models, we show simulations for magnetic filling factors of  $f = 0.1$ ,  $0.01$  and  $0.001$  per cent.

In the upper parts of the tube atmospheres, the temperatures in the model with the widest tube opening radius are expected to be lowest due to the largest dilution of the wave energy flux. The difference in dilution is expected to be a factor of 100 between  $f = 0.1$  and  $0.001$  per cent; however, it is significantly lower, i.e. a factor of between 3 and 26 for models with or without time-dependent ionization and with or without the consideration of LTW frequency spectra (see Tables 3 and 4). For some portions of the tube atmospheres, it is even found that ‘the larger the tube opening radius, the higher the mean temperatures’, a result that is highly counterintuitive. The reason for this behaviour is that the dilution of the wave energy flux does not exactly follow geometrical scaling. Other relevant processes involve the density structure within the flux tubes as well as significant dynamical and radiative processes, especially pertaining to strong shocks, including significant radiative energy losses. Comparing models with and without time-dependent ionization reveals that time-dependent ionization leads to lower average temperatures inside the flux tubes compared to time-independent ionization. However, the average temperatures inside of flux tubes in models with or without time-dependent ionization are nonetheless noticeably higher than in the acoustically heated external atmosphere, pointing to the significance of magnetic heating.

We also pursued corresponding sets of models based on LTW frequency spectra instead of monochromatic waves. In this type of models the attained time-averaged temperatures were unrealistically low, particularly in models of time-dependent ionization. In this case, the combined effects of time-dependent hydrogen ionization and of the dynamical structure related to the propagation of spectral waves lead to very strong shocks, which invoked amplified energy losses behind the shocks as well as strong atmospheric

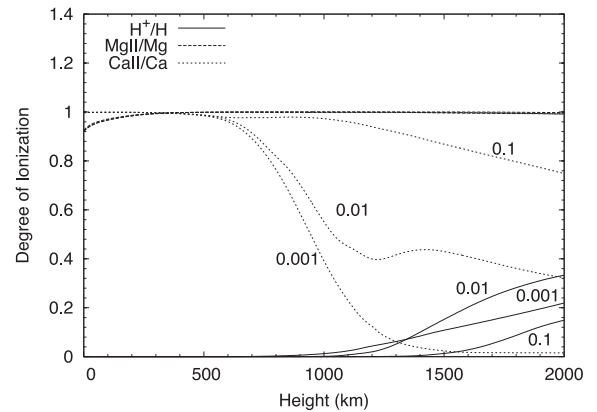


**Figure 8.** Comparison of the time-averaged ionization degrees for hydrogen, magnesium and calcium concerning longitudinal wave computations with time-dependent ionization and with consideration of frequency spectra. We depict results for magnetic flux tubes with filling factors of  $f = 0.1$ ,  $0.01$  and  $0.001$  per cent.

expansions associated with quasi-adiabatic cooling, see e.g. Gail, Cuntz & Ulmschneider (1990) and Koninx & Pijpers (1992) for theoretical work on the build-up of wave pressure due to shocks. The impact of very strong shocks entailed that the time-averaged temperatures are lowest in models of small tube spreading, i.e. high magnetic filling factors (e.g. case of  $f = 0.1$  per cent) if time-dependent ionization of hydrogen is taken into account.

Finally, we studied the behaviour of the height-dependent time-averaged hydrogen ionization in our set of models (see Figs 8

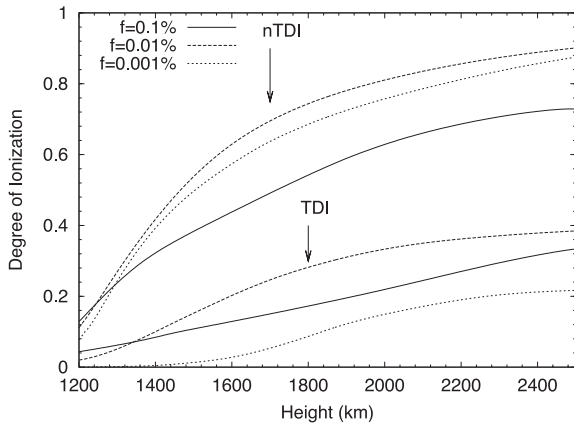


**Figure 9.** Comparison of time-averaged hydrogen ionization degrees for longitudinal wave computations with (TDI) and without (nTDI) time-dependent ionization regarding models based on frequency spectra. We depict results for magnetic flux tubes with filling factors of  $f = 0.1, 0.01$  and  $0.001$  per cent.

and 9). We found that the hydrogen ionization degrees steadily increase at heights beyond 1200 km regardless of the magnetic filling factor, i.e. the tube top opening radius. However, in general, they remain relatively low (i.e. below 40 per cent) in models with time-dependent ionization (TDI), whereas they are relatively high (i.e. between 70 and 90 per cent at heights beyond 2000 km) in models without time-dependent ionization (nTDI). This is consistent with the general behaviour of time-dependent hydrogen ionization as described, as in this case lower degrees of ionization occur at most heights, especially in regions behind shocks, including regions of strong shocks owing to the time-delay of ionization in accord to the time-dependent statistical rate equations (see Section 2.1).

We also evaluated time-dependent effects for the ionization of calcium and magnesium (see Fig. 8), noting that  $\text{Ca II}$  and  $\text{Mg II}$  are of significant importance for the facilitation of radiative cooling (see Section 2.2). Our simulations show that most of the magnesium is ionized to  $\text{Mg II}$  at most heights regardless of the geometrical filling factor of the respective flux tube. However, for  $\text{Ca II}$  the height-dependent behaviour of the ionization degree is strongly impacted by the geometrical spread of the flux tubes (see Fig. 2). Generally, for smaller values of  $f$ , associated with a lesser dilution of the wave energy flux, a larger fraction of calcium is ionized to  $\text{Ca II}$ . The reason for this behaviour is the lower dilution of the wave energy flux in those models, leading to more effective shock heating and higher overall temperatures.

#### 4 SUMMARY AND CONCLUSIONS

We pursued sets of time-dependent model simulations for solar magnetic flux tubes with focus on LTW with and without the consideration of time-dependent ionization, particularly pertaining to hydrogen. The treatment of LTW is motivated by a large variety of studies including work by Hasan & van Ballegoijen (2008) arguing that LTW are able to provide quasi-steady heating sufficient to explain the bright solar network grains observed in  $\text{Ca II H}$  and  $\text{K}$ . We studied the dynamics of flux tubes with different magnetic filling factors, i.e. 0.1, 0.01 and 0.001 per cent, corresponding to different tube top opening radii, guided and motivated by previous observational results (e.g. Spruit & Roberts 1983; Solanki 1996). It was found that the dynamic tube structures are determined by a complex interplay between shock heating, radiative and hydrodynamic

cooling (with the latter caused by wave pressure), dilution of the wave energy flux due to the flux tube geometry and time-dependent ionization. We identified pronounced differences between the tube models especially in regard to tubes with different tube opening radii and in response to the inclusion or omission of time-dependent ionization.

Similar to the case of acoustic waves, time-dependent ionization in LTW models leads to a large range of phenomena, such as over- and underionization of the flow, increased temperature jumps at shocks, and modified mean (i.e. time-averaged) temperature, density and ionization structures. The impact of time-dependent treatment of ionization for flux tubes becomes evident through comparisons of mean temperatures between the different types of models. Regarding monochromatic models it was found that time-dependent ionization leads to lower average temperatures inside flux tubes compared to time-independent ionization, an effect already known for acoustically heated models.

However, the average temperatures inside of flux tubes in models with and without time-dependent ionization are nonetheless noticeably higher than in the acoustically heated external atmosphere. If monochromatic LTW are used, the mean (i.e. time-averaged) temperatures of the tubes generally show a quasi-steady increase with height. However, if frequency spectra are used, the mean temperatures, in essence, show no rise with height at all. This behaviour is initiated by the formation of very strong shocks (especially in narrow tubes, corresponding to small magnetic filling factors) resulting in large-scale quasi-adiabatic cooling, leading to unrealistically low temperatures. This type of result has already previously been found in corresponding 1D models of acoustic waves (e.g. Carlsson & Stein 1992, 1995; Rammacher & Ulmschneider 2003), a behaviour deemed highly unrealistic (Ulmschneider et al. 2005).

An appropriate enhancement of our current models will be the calculation of self-consistent 3D MHD models. Those models face, however, the principal challenge of the necessity to include both detailed multilevel 3D radiative transfer and 3D flows including the detailed treatment of shock formation and shock interaction. Important progress has already been made (e.g. Stein et al. 2009a,b), but further efforts are needed to obtain of a concise picture. Tentative insights into the principal properties of these types of future models can be attained through inspecting existing 3D time-dependent *non-magnetic* hydrodynamics models, which also consider time-dependent non-equilibrium effects caused by hydrogen (Leenaarts & Wedemeyer-Böhm 2006), albeit various restrictive assumptions including (but not limited to) the lack of back-coupling of the ionization to the equation of state. In this type of models it is found that the build-up of strong shocks due to shock interaction is largely absent, resulting in a lack of unrealistically high cooling behind the strong shocks previously also referred to as ‘hydrodynamic refrigeration’ (Cuntz & Muchmore 1994). In this case a quasi-steady rise of temperature with height is attained, which appears to be in close resemblance to empirical solar chromosphere models (e.g. Anderson & Athay 1989). Nonetheless, our results based on time-dependent ionization and LTW frequency spectra allow insight into the limiting case of 1D geometry, while also noting that our models based on time-dependent ionization and monochromatic waves are expected to be approximately reflective of physical reality.

An alternative, or perhaps supplementary, way of supplying chromospheric heating might be given through ambipolar diffusion as described by Khomenko & Collados (2012). Here the presence of neutrals, together with the decrease with height of the collisional coupling, leads to deviations from the classical magnetohydrodynamic behaviour of the chromospheric plasma. Khomenko &

Collados (2012) pointed out that a relative net motion occurs between the neutral and ionized components, referred to as ambipolar diffusion. According to this model, the dissipation of currents in the chromosphere is enhanced by orders of magnitude due to the action of ambipolar diffusion, as compared with the standard ohmic diffusion. The authors proposed that a significant amount of magnetic energy can be released to the chromosphere just by existing force-free 10–40 G magnetic fields there.

Additional studies were given by Fedun, Erdélyi & Shelyag (2009), Vigeesh, Hasan & Steiner (2009) and Erdélyi & Fedun (2010). Fedun et al. (2009) studied the oscillatory response of the 3D solar photosphere to the leakage of photospheric motion. They found, among other results, that high-frequency waves propagate from the lower atmosphere across the transition region experiencing relatively low reflection, and transmitting most of their energy into the corona, and, furthermore, that the magnetic field acts as a waveguide for both high- and low-frequency waves originating from the photosphere and propagating up into the solar corona. Vigeesh et al. (2009) provided a targeted study on wave propagation and energy transport in the magnetic network of the Sun based on 2D MHD simulations, which among other results identified the limited capacity of acoustic waves. Erdélyi & Fedun (2010) investigated the oscillatory modes of a magnetically twisted compressible flux tube embedded in a compressible magnetic setting, including applications to solar magneto-seismology.

As an overarching statement concerning our study we conclude that the significance of time-dependent ionization identified in the simulations of LTW is a stark motivation to also consider this type of effect in future models of transverse and torsional tube waves. This will allow us to obtain a more detailed picture of the dynamics and energetics of solar-type outer atmospheres. This obvious suggestion is also supported by the repeatedly obtained finding that longitudinal flux tube waves, as gauged through models considering time-dependent ionization phenomena as done in the present study, are insufficient to supply an adequate amount of energy for balancing coronal heating in the view of early and updated estimates by Güdel (2007) and others.

## ACKNOWLEDGMENTS

This work utilizes an OHD-MHD computer code package developed by P. Ulmschneider and his group (which also included the authors of this study) at the Institute for Theoretical Astrophysics, University of Heidelberg, Germany, including subsequent augmentations.

## REFERENCES

Anderson L. S., Athay R. G., 1989, *ApJ*, 346, 1010  
 Avrett E. H., 1985, in Lites B. W., ed., *Chromospheric Diagnostics and Modelling*. NSO, Sacramento Peak, p. 67  
 Beck C. A. R., Rammacher W., 2010, *A&A*, 510, A66  
 Beck C., Rezaei R., Puschmann K. G., 2012, *A&A*, 544, A46  
 Bello González N., Flores Soriano M., Kneer F., Okunev O., 2009, *A&A*, 508, 941  
 Bogdan T. J. et al., 2003, *ApJ*, 599, 626  
 Bohn H. U., 1984, *A&A*, 136, 338  
 Bruls J. H. M. J., Solanki S. K., 1993, *A&A*, 273, 293  
 Carlsson M., Stein R. F., 1992, *ApJ*, 397, L59  
 Carlsson M., Stein R. F., 1995, *ApJ*, 440, L29  
 Carlsson M., Stein R. F., 2002, *ApJ*, 572, 626  
 Castelli F., Kurucz R. L., 2004, in Piskunov N. E., Weiss W. W., Gray D. F., eds, *Proc. IAU Symp. 210, Stars as Suns: Modelling of Stellar*

*Atmospheres*. Astron. Soc. Pac., San Francisco, CD-ROM, Poster 20 preprint (arXiv:astro-ph/0405087)  
 Cuntz M., 1987, *A&A*, 188, L5  
 Cuntz M., 2004, *A&A*, 420, 699  
 Cuntz M., Muchmore D. O., 1994, *ApJ*, 433, 303  
 Cuntz M., Suess S. T., 2004, *A&A*, 424, 1003  
 Cuntz M., Ulmschneider P., 1988, *A&A*, 193, 119  
 Cuntz M., Rammacher W., Ulmschneider P., Musielak Z. E., Saar S. H., 1999, *ApJ*, 522, 1053  
 Cuntz M., Rammacher W., Musielak Z. E., 2007, *ApJ*, 657, L57  
 Erdélyi R., Ballai I., 2007, *Astron. Nachr.*, 328, 726  
 Erdélyi R., Fedun V., 2010, *Sol. Phys.*, 263, 63  
 Fawzy D. E., 2010, *MNRAS*, 408, 293  
 Fawzy D. E., Cuntz M., 2011, *A&A*, 526, A91  
 Fawzy D. E., Ulmschneider P., Cuntz M., 1998, *A&A*, 336, 1029  
 Fawzy D. E., Rammacher W., Ulmschneider P., Musielak Z. E., Stępień K., 2002, *A&A*, 386, 971  
 Fedun V., Erdélyi R., Shelyag S., 2009, *Sol. Phys.*, 258, 219  
 Fossum A., Carlsson M., 2005, *Nat*, 435, 919  
 Gail H.-P., Cuntz M., Ulmschneider P., 1990, *A&A*, 234, 359  
 Güdel M., 2007, *Living Rev. Sol. Phys.*, 4, 3  
 Gudiksen B. V., Carlsson M., Hansteen V. H., Hayek W., Leenaarts J., Martínez-Sykora J., 2011, *A&A*, 531, A154  
 Hasan S. S., van Ballegooijen A. A., 2008, *ApJ*, 680, 1542  
 Herbold G., Ulmschneider P., Spruit H. C., Rosner R., 1985, *A&A*, 145, 157  
 Kalkofen W., 2007, *ApJ*, 671, 2154  
 Khomeiko E., Collados M., 2012, *ApJ*, 747, 87  
 Klimchuk J. A., 2006, *Sol. Phys.*, 234, 41  
 Koninx J.-P. M., Pijpers F. P., 1992, *A&A*, 265, 183  
 Leenaarts J., Wedemeyer-Böhm S., 2006, *A&A*, 460, 301  
 Lighthill M. J., 1978, *Waves in Fluids*. Cambridge Univ. Press, Cambridge  
 Linsky J. L., 1991, in Ulmschneider P., Priest E. R., Rosner R., eds, *Mechanisms of Chromospheric and Coronal Heating*. Springer, Berlin, p. 166  
 Mihalas D., Mihalas B. W., 1984, *Foundations of Radiation Hydrodynamics*. Oxford Univ. Press, New York  
 Musielak Z. E., 2004, in Dupree A. K., Benz A. O., eds, *Proc. IAU Symp. 219, Stars as Suns: Activity, Evolution and Planets*. Astron. Soc. Pac., San Francisco, p. 437  
 Musielak Z. E., Rosner R., Stein R. F., Ulmschneider P., 1994, *ApJ*, 423, 474  
 Narain U., Ulmschneider P., 1996, *Space Sci. Rev.*, 75, 453  
 Nieuwenhuijzen H., de Jager C., Cuntz M., Lobel A., Achmad L., 1993, *A&A*, 280, 195  
 Ofman L., Nakariakov V. M., DeForest C. E., 1999, *ApJ*, 514, 441  
 Ofman L., Nakariakov V. M., Sehgal N., 2000, *ApJ*, 533, 1071  
 Rammacher W., Cuntz M., 2003, *ApJ*, 594, L51  
 Rammacher W., Cuntz M., 2005a, in Favata F., Hussain G. A. J., Battrick B., eds, *Cool Stars, Stellar Systems, and the Sun 13*. ESA SP-560, Vol. II, p. 891  
 Rammacher W., Cuntz M., 2005b, *A&A*, 438, 721  
 Rammacher W., Ulmschneider P., 2003, *ApJ*, 589, 988  
 Rammacher W., Fawzy D. E., Ulmschneider P., Musielak Z. E., 2005, *ApJ*, 631, 1113  
 Rammacher W., Ulmschneider P., 1989, in Rutten R. J., Severino G., eds, *Solar and Stellar Granulation*. Kluwer, Dordrecht, p. 589  
 Roberts B., 2004, in Lacoste H., ed., *SOHO 13: Waves, Oscillations and Small-Scale Transient Events in the Solar Atmosphere: A Joint View of SOHO and TRACE*. ESA SP-547, p. 1  
 Schmitz F., Ulmschneider P., Kalkofen W., 1985, *A&A*, 148, 217  
 Schrijver C. J., 2001, *ApJ*, 547, 475  
 Schrijver C. J., Zwaan C., 2000, *Solar and Stellar Magnetic Activity*. Cambridge Univ. Press, Cambridge  
 Solanki S. K., 1993, *Space Sci. Rev.*, 63, 1  
 Solanki S. K., 1996, in Strassmeier K. G., Linsky J. L., eds, *Proc. IAU Symp. 176, Stellar Surface Structure*. Kluwer, Dordrecht, p. 201  
 Solanki S. K., Roberts B., 1992, *MNRAS*, 256, 13  
 Spruit H. C., Roberts B., 1983, *Nat*, 304, 401  
 Steffen M., 1993, *Habilitation thesis*, Univ. Kiel, Germany

- Stein R. F., Nordlund Å., Georgobiani D., Benson D., Schaffenberger W., 2009a, in Dikpati M., Arentoft T., González Hernández I., Lindsey C., Hill F., eds, ASP Conf. Ser. Vol. 416, Solar–Stellar Dynamos as Revealed by Helio- and Asteroseismology. Astron. Soc. Pac., San Francisco, p. 421
- Stein R. F., Georgobiani D., Schaffenberger W., Nordlund Å., Benson D., 2009b, in Stempels E., ed., AIP Conf. Proc. Vol. 1094, Cool Stars, Stellar Systems, and the Sun 15. Am. Inst. Phys., New York, p. 764
- Stenflo J. O., 1978, Rep. Progress Phys., 41, 865
- Trampedach R., Christensen-Dalsgaard J., Nordlund Å., Stein R. F., 1997, in Pijpers F. P., Christensen-Dalsgaard J., Rosenthal C. S., eds, Solar Convection and Oscillations and their Relationship. Kluwer, Dordrecht, p. 73
- Ulmschneider P., Musielak Z. E., 1998, A&A, 338, 311
- Ulmschneider P., Musielak Z., 2004, in Pevtsov A. A., Uitenbroek H., eds, ASP Conf. Ser. Vol. 286, Current Theoretical Models and Future High Resolution Solar Observations: Preparing for ATST. Astron. Soc. Pac., San Francisco, p. 363
- Ulmschneider P., Kalkofen W., Nowak T., Bohn U., 1977, A&A, 54, 61
- Ulmschneider P., Theurer J., Musielak Z. E., 1996, A&A, 315, 212
- Ulmschneider P., Musielak Z. E., Fawzy D. E., 2001, A&A, 374, 662
- Ulmschneider P., Rammacher W., Musielak Z. E., Kalkofen W., 2005, ApJ, 631, L155
- Vernazza J. E., Avrett E. H., Loeser R., 1981, ApJS, 45, 635
- Vigeesh G., Hasan S. S., Steiner O., 2009, A&A, 508, 951
- Wedemeyer-Böhm S., Scullion E., Steiner O., van der Voort L. R., de la Cruz Rodríguez J., Fedun V., Erdélyi R., 2012, Nat, 486, 505
- Worrall G., 2012, Sol. Phys., 279, 43

This paper has been typeset from a  $\text{\TeX}/\text{\LaTeX}$  file prepared by the author.